Solar Energy Materials & Solar Cells 279 (2025) 113257

Contents lists available at ScienceDirect

Solar Energy Materials and Solar Cells

journal homepage: www.elsevier.com/locate/solmat

Two-step nested optical-electrical Monte-Carlo approach to analyze the influence of tolerances on Micro-CPV module performance

Elisa Kaiser [a,b,*], Maike Wiesenfarth [a], Peter Schöttl [a], Marc Steiner [a], Stefan W. Glunz [a,b], Henning Helmers [a]

[a] Fraunhofer Institute for Solar Energy Systems ISE, 79110, Freiburg, Germany
[b] Chair for Photovoltaic Energy Conversion, University of Freiburg, Emmy-Noether-Str. 2, 79110, Freiburg, Germany

ARTICLE INFO

Keywords:
Micro-concentrator photovoltaics
Nested Monte-Carlo simulation
Tolerances
Electrical interconnection
Angle of incidence
Ray tracing

ABSTRACT

In manufacturing and product optimization, understanding the influence of tolerances, which are inevitable variations in production processes, is crucial for enhancing performance while managing costs. However, previous analytical approaches lacked the capability to quantitatively assess the cumulative effect of multiple tolerances due to their random combination and statistical independence. In this work, we introduce a novel method that overcomes these limitations by effectively modeling complex dependencies among tolerances through a two-step nested Monte-Carlo approach. We apply this model to a micro-CPV module developed at Fraunhofer ISE. First, we randomly select and combine tolerances in a cell-lens unit using ray tracing. Then, we randomly select and combine these units in a full 690-cell module using an electrical network model considering different angles of incidence. The considered tolerances include deviations in component geometries and displacements and are based on measurements. The model predicts the acceptance angle and allows to identify the optimal interconnection schemes. Further, it is capable to determine the maximum tolerances permissible for maintaining a certain module power. While tolerances lead to a distribution in current generation among the cell-lens units, we find that parallel interconnections can compensate for such variations. Further, we identify that the positions of secondary lens and micro solar cell are the most sensitive parameters for achieving high module power. These findings are crucial for refining module design cost-effectively. Moreover, the model facilitates a quantitative assessment of optimization potentials, guiding decision-making in product development and manufacturing, and a techno-economic optimization.

1. Introduction

Micro-concentrator photovoltaic (micro-CPV) approaches promise to revolutionize CPV technology. High sunlight concentration ratios around 1000 combined with the miniaturization of components, the adaptation of parallelized and high-throughput processes from other industries, which leverage additive manufacturing and self-assembly, yield a roadmap towards significant reduction of the levelized cost of electricity for micro-CPV [1–5]. However, miniaturization is challenged by tolerances of all components and processes, which generally are given as absolute deviations from the nominal values and, thus, become relatively larger for smaller components. Due to the high concentration ratio even minor deviations from the optimal alignment can direct solar radiation away from the active solar cell surface, leading to dropping optical efficiency and performance losses.

In our micro-CPV module, each cell-lens unit comprises a primary optical element (POE) that focuses light onto a secondary optical element (SOE), which captures the light and directs it onto the micro solar cell. Within this assembly, both component and manufacturing tolerances are present. Component tolerances refer to deviations in the geometry, such as the shape or size of the components, while manufacturing tolerances refer to deviations in the positioning and alignment of the components within a single cell-lens unit.

The relationship between tolerances and the current generation of cell-lens units is complex due to the random combination of component and manufacturing tolerances, resulting in a vast number of possible combinations. Individual combinations of tolerances and their impact on the current generation of single cell-lens units have been modeled [6–8], but assessing all potential combinations through a comprehensive parameter study requires excessive computational resources and seems

* Corresponding author. Fraunhofer Institute for Solar Energy Systems ISE, 79110, Freiburg, Germany.
E-mail address: elisa.kaiser@ise.fraunhofer.de (E. Kaiser).

https://doi.org/10.1016/j.solmat.2024.113257
Received 28 June 2024; Received in revised form 23 September 2024; Accepted 24 October 2024
Available online 2 November 2024

practically impossible. Consequently, the adoption of a statistical approach is crucial.

In a separate publication [9], we introduced a Monte-Carlo based approach in which we combine various tolerances in a statistical manner to study their effects on the current generation of individual cell-lens units using an optical ray tracing model and, subsequently, the acceptance angle. The tolerances were derived from measurements on prototype components and modules.

In this work, we extend the Monte-Carlo approach for single cell-lens units by a second nested Monte-Carlo step to study the impact of tolerances at the module level. As tolerances result in a distribution of photo currents, the interconnection scheme within a micro-CPV module, being in series, in parallel, or a combination of the two, can impact the power output of full modules. Steiner et al. [10] analyzed different electrical combination strategies for CPV modules. Depending on the electrical interconnection, the losses of individual cells can be compensated or exacerbated.

A central question addressed in this research is identifying advantageous electrical interconnection strategies that adapt to the specific current distributions among individual cells. Additionally, we study the influence of different tolerances quantitatively and for different incidence angles, considering the relevance of precise solar tracking.

The article is organized as follows: First, we introduce the general simulation approach, including the simulation process, application of the method to our micro-CPV module, and validation through comparison with experimental data. Then, we apply the model to assess the impact of different tolerance distributions, as reported in Ref. [9], on the power output of full modules. Different interconnection schemes are analyzed using an electrical network model. Finally, we perform a sensitivity analysis to determine the maximum tolerances permissible for maintaining a certain module power.

2. Two-step nested optical-electrical Monte-Carlo approach

2.1. Simulation process

Fig. 1 shows a flowchart of the two-step nested optical-electrical Monte-Carlo model. As a first step, a single cell-lens unit is modeled by ray tracing using the in-house software "Raytrace3D" [11,12] as discussed in detail elsewhere [9]. Here, the specification of POE and SOE, including their geometry and materials, as well as the solar cell receiver are defined. The sun as illumination source is defined by its spectral distribution, sun shape and circumsolar radiation. To accommodate possible misalignments of the module on the tracking unit and actual tracking errors, the alignment of the cell-lens unit surface relative to the sun is incorporated as an independent variable, referred to as angle of incidence (*AOI*). Tolerances, i.e. deviations from the design case in terms of component size, shape, and relative positions, are addressed as follows: Each tolerance is represented by a statistical distribution that reflects deviations from the design case due to actual component manufacturing and module assembly. Employing the Monte-Carlo technique, a multitude of N cell-lens units diverging from the design case is generated through random selection from these weighted tolerance distributions.

The ray tracing yields the spectrally and spatially resolved irradiance distribution $P_{PV}(x,y,\lambda)$ across the solar cell receiver (*PV*). Integration over wavelength λ yields the spatially resolved irradiance distribution $P_{PV}(x,y)$, which is also referred to as the flux profile. The photogenerated currents $I_{ph,i}$ for each subcell i of a multi-junction solar cell are calculated using the spectrally resolved irradiance distribution $P_{PV}(\lambda)$ and the external quantum efficiency ($EQE_i(\lambda)$):

$$I_{ph,i} = \int_{\lambda_{i1}}^{\lambda_{i2}} P_{PV}(\lambda)\frac{q\lambda}{hc}EQE_i(\lambda)d\lambda \tag{1}$$

With the elementary charge q, Planck's constant h, and speed of light in vacuum c.

The second step models the current-voltage characteristics of a full module based on the subcell current distributions of the single cell-lens units using the electrical network solver "LTspice" from Linear Technologies [13].

In the SPICE network we model the multi-junction solar cell as i subcells represented by two-diode models with subcell current sources, and a lumped resistance (see Fig. 1, sketch within the "Cell structure" box). The lumped resistance includes the front grid fingers, sheet resistance and vertical conduction, as well as cell interconnection inside of the micro-CPV module. The diodes account for recombination in both the neutral and depletion regions, characterized by saturation current densities ($J_{01,i}$, $J_{02,i}$) and an exponential function. The current source represents the short-circuit current density of the solar cell $J_{sc,i}$, which is determined in the first step of the Monte-Carlo approach. The

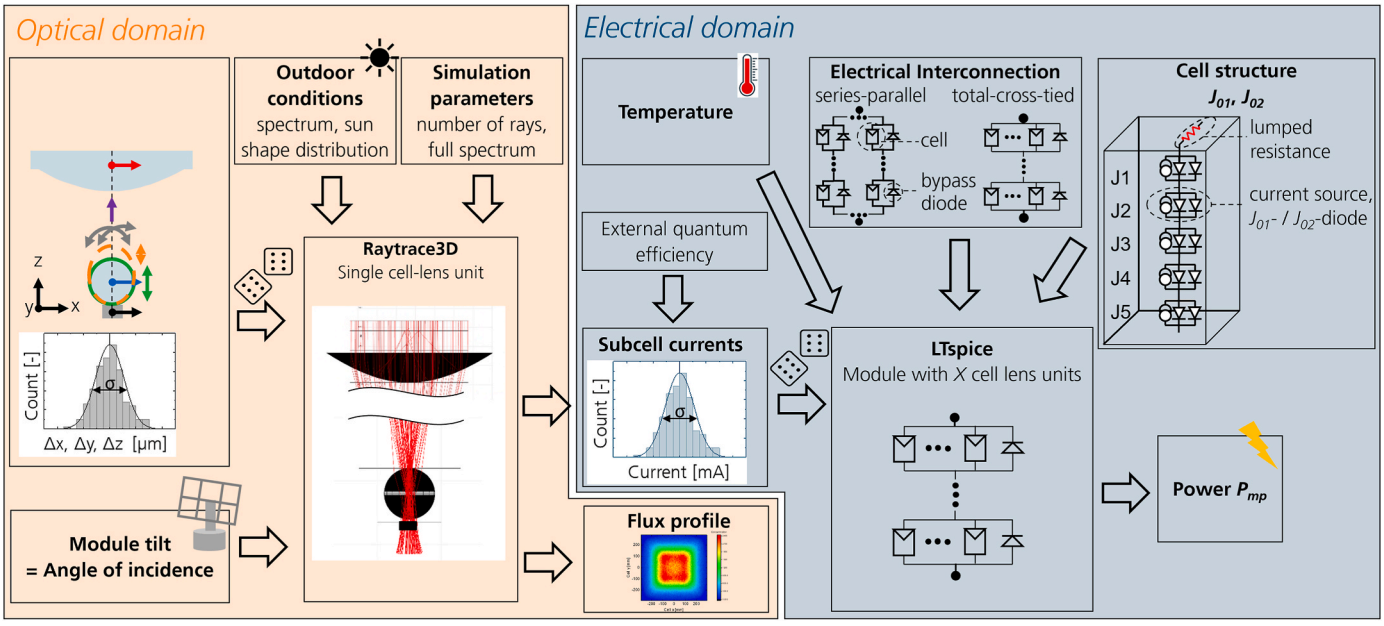

Fig. 1. Flowchart of the two-step nested optical-electrical Monte-Carlo method.

parameters $J_{01,i}$, $J_{02,i}$ and $J_{sc,i}$ vary with temperature. The temperature dependence of $J_{sc,i}(T)$ is assessed using temperature dependent *EQE* data, while $J_{01,i}(T)$ and $J_{02,i}(T)$ are calculated as follows [14]:

$$J_{01,i}(T) = k_{01,i} T^3 \, exp\left[-\frac{E_{g,i}(T) - \Delta E_{g,i}}{k_B T} \right] \quad (2)$$

$$J_{02,i}(T) = k_{02,i} T^{2.5} \, exp\left[-\frac{E_{g,i}(T) - \Delta E_{g,i}}{2 k_B T} \right] \quad (3)$$

With the temperature dependent bandgap energy $E_{g,i}(T)$, Boltzmann's constant k_B and three fitting parameters $k_{01,i}$, $k_{02,i}$ and $\Delta E_{g,i}$ that are extracted by fitting of measured *J-V* curves of the multi-junction solar cell. $E_{g,i}(T)$ is determined fitting the relationship introduced by Varshni et al. [15] to $E_{g,i}(T)$ data. $E_{g,i}(T)$ is derived from temperature dependent subcell *EQE* measurements after the procedure introduced by Helmers et al. [16]. Note that a uniform temperature is assumed across the entire module, tunnel diodes are modeled as ideal resistors contributing to the lumped resistance, and the parallel resistance is assumed to be of negligible influence and thus idealized as infinity.

The electrical interconnection of the solar cells is either series-parallel (SP) or in a total-cross-tied (TCT) configuration, as illustrated in Fig. 1 within the box "Electrical interconnection". Each parallel group includes a bypass diode connected in parallel. A series resistance in the connection between two cells is neglected.

In the second Monte-Carlo step, each subcell current combination is randomly selected from the statistical distribution resulting from the ray tracing. Then, we simulate the *I-V* characteristics of a module and determine the maximum power output. Repetition of this procedure yields a statistical distribution.

2.2. Application of the method

2.2.1. Simulation input

The optical modeling is described in detail in Ref. [9]: The ray tracing simulation of the single cell-lens units is conducted with the solar reference spectrum AM1.5d ASTM G173–03:2008 [17], for a wavelength range of 280 nm–1980 nm with spectral resolution of 10 nm. The sun shape distribution and circumsolar radiation are based on the data by Neumann et al. [18]. At each wavelength step, the ray density is 10 rays/mm^2 impinging on the primary aperture. Repeating the same analysis with this ray density ten times results in a maximum deviation in current of $\pm 0.29\%_{rel}$. The solar cell receiver is discretized with 100 × 100 bins, each representing an area of 5.85 × 5.85 μm^2. The angle of incidence is adjusted from 0° to 0.8° in increments of 0.1°.

The *EQE* of the five-junction (5J) solar cells used is similar to those of the five-junction 5C46 by AZUR SPACE as presented in Ref. [19]. The temperature dependent saturation current densities $J_{01,i}(T)$ and $J_{02,i}(T)$ and the fit parameters $k_{01,i}$, $k_{02,i}$ and $\Delta E_{g,i}$ are derived from fitting *I-V* curves of 5J solar cells measured at various temperatures. The assumed operating temperature for all cells in the module is 90 °C.

2.2.2. Micro-CPV module

In the following, the micro-CPV module developed at Fraunhofer ISE [1,6,20] is introduced and the relevant tolerances are described.

The cell-lens unit consists of 5J solar cell with an edge length of 585 μm, a spherical lens as secondary optical element with a diameter of 1.6 mm and a plano-convex silicone-on-glass lens as primary optical element with an edge length of 18.5 mm. The focal distance is 44 mm. In the following, a cell-lens unit comprising ideal components of the specified sizes and exhibiting ideal alignment is referred to as design case. The target module is based on a panel-sized base plate (24" × 18"), consists of 690 cell-lens units and has an aperture area of 0.236 m^2.

Eight different tolerances relating to the size, shape and alignment of different components are considered, as illustrated in Fig. 2: lateral displacements (*x,y*) of cell, SOE, and POE, vertical displacement between the base plate and POE (height *z*), the deviation in the SOE diameter (SOE *d*), the SOE roundness (SOE *a*), the tilt of the SOE (δ_{soe}) and the direction of the tilted SOE ($\phi_{\delta soe}$). The SOE roundness is defined as the ratio of the radius in the vertical direction (r_1) to the equatorial radius (r_2) of the sphere. In this context, SOE *a* represents the extension or contraction of the radius in the vertical direction ($r_1/r_2 = (r_2 + a)/r_2$)).

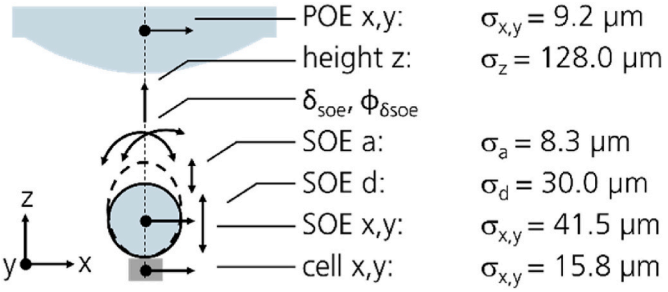

Fig. 2. Not-to-scale sketch of a cell-lens unit of the micro-CPV module with the deviations from ideal (arrows) and the standard deviations σ of the measured tolerances, i.e. reference case. Sketch adapted from Ref. [9].

Tolerance distributions were determined based on experimental data from fabricated micro-CPV prototype modules consisting of 3 × 3 and 10 × 6 cell-lens units. The lateral displacements of the cell, SOE and POE and the vertical displacements of the POE to the base plate are measured using a coordinate measurement device (accuracy <2 μm). SOE diameter and roundness were measured by the manufacturer.

Normal distributions are fitted to the measured data with values listed in Fig. 2. The tilt of the SOE δ_{soe} and the direction of the tilted SOE $\phi_{\delta soe}$ are uniformly distributed. In the following, the tolerance distributions based on the measured data are referred to as reference case.

The first step of the model is used to calculate the subcell currents of the cell-lens units across various *AOIs*. For each *AOI, N* different geometries are modeled selected with Monte-Carlo tolerance statistics. A convergence study demonstrated that after 1000 iterations, the deviation in median current for additional *N* remains below 0.1 % [9]. The second step is used to calculate the power of modules. For each *AOI*, *M* different modules are simulated, with the currents selected using Monte-Carlo statistics. For $M = 500$, the deviation in median power is maintained below 0.1 % with further iterations.

2.3. Validation of the model

The validation involves comparing module measurements with known deviations, with corresponding simulations that also integrate these deviations. Outdoor measurement results of three different modules (A, B, C) are used to validate the nested optical-electrical model, namely by comparing acceptance angle measurements with simulation. Each module contains nine 5J solar cells interconnected in a TCT configuration. Three solar cells are connected in parallel, and these groups are then connected in series. Each parallel group is also equipped with a bypass diode. For the three modules the positions of the SOEs have been displaced on purpose in different manner.

The three modules were measured on the outdoor CPV test tracker at Fraunhofer ISE in Freiburg, Germany (see Fig. 3).

After module assembly, the lateral cell, SOE and POE positions, the distance between POE and base plate, and the SOE diameter were precisely measured for each cell-lens unit. Note that the SOE roundness and tilt could not be measured individually. The measured tolerances of all components closely align with those of the reference case, with the exception for the SOE position, which was varied on purpose. The mean radial displacement is $r_{SOE,mean}$ = 20 μm, 115 μm, and 237 μm for modules A, B, and C, respectively.

Each cell-lens unit within the 3 × 3 array is simulated using ray

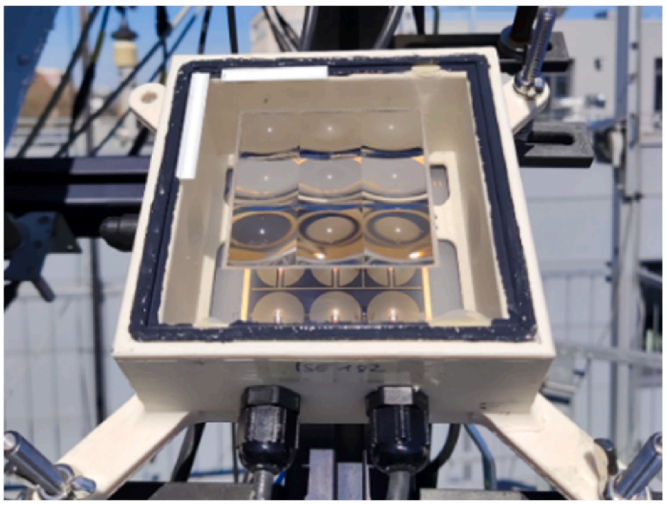

Fig. 3. Photograph of the micro-CPV prototype module A with a 3 × 3 array of cell-lens units, mounted on the outdoor CPV test tracker at Fraunhofer ISE, Freiburg.

tracing, incorporating the measured positions and sizes of the components. Subsequently, the calculated subcell currents from the nine cells are electrically interconnected using LTspice and the *I-V* characteristic of the module is modeled.

Fig. 4 shows the simulated (open symbols, dashed line) and measured (closed symbols, solid line) normalized power output P_{mp} plotted against the angle of incidence.

The acceptance angles $\alpha_{90\%,Pmp}$, defined as the half module tilt angle relative to the aperture plane until which 90 % of the maximum power output is maintained, are listed in Table 1. The deviation between measured and modeled $\alpha_{90\%,Pmp}$ is below 0.07°. Module C (blue, circle) with the largest tolerances has the smallest $\alpha_{90\%,Pmp}$, while module A (green, triangle) with the most precise tolerances, exhibits the largest $\alpha_{90\%,Pmp}$. Note that this agreement is achieved despite the lack of fine-tuning for e.g. spectral conditions and exact temperatures. The direct normal irradiance (*DNI*) ranged from 817 to 945 W/m^2 and the ambient temperature T_{amb} varied between 9 °C and 27 °C. The spectral conditions, with spectral matching ratio (SMR_{ij}) values for a triple-junction solar cell as specified by IEC 62670–3 [21] of $SMR_{12} = 1 \pm 0.03$, $SMR_{13} = 1 \pm 0.08$ and $SMR_{23} = 1 \pm 0.08$, differ from the simulated AM1.5d spectrum.

We conclude that the combination of optical ray tracing and electrical SPICE model reproduces measurements well and, thus, is considered to be validated.

Table 1
Comparison of the acceptance angles required to achieve 90 % of the maximum P_{mp} ($\alpha_{90\%,Pmp}$) between measurements on the outdoor tracker at Fraunhofer ISE and optical-electrical simulations for three different modules.

Module	$r_{soe,mean}$ [µm]	$\alpha_{90\%,Pmp}$ [°]	
		Measured	Modeled
A	20	0.62	0.69
B	115	0.56	0.55
C	237	0.25	0.28

3. Results and discussion

3.1. Influence of measured tolerances on the module performance

In the following, we apply the model to study how the interconnection scheme impacts the performance, i.e. P_{mp} and acceptance angle of the target module consisting of 690 cell-lens units and a geometrical concentration of 1000X.

3.1.1. Electrical interconnection

Solar cells within a module generate statistically distributed currents due to tolerances. To study the potential of electrical interconnection to mitigate losses, we implemented different interconnection schemes into our model following the procedure of Steiner et al. [10]. Two electrical configurations are compared: series-parallel and total-cross-tied configuration. In SP configuration, solar cells are connected in series to form strings and the strings are connected in parallel to each other. In TCT configuration, the solar cells are first connected in parallel, and these groups are then connected in series. Each parallel group includes a bypass diode, as illustrated in Fig. 1, box "Electrical interconnection".

At $AOI = 0°$, we find that the impact of the electrical interconnection on the power output of the module is very low. In this case, even with tolerances for almost all combinations, the concentrated light spot still

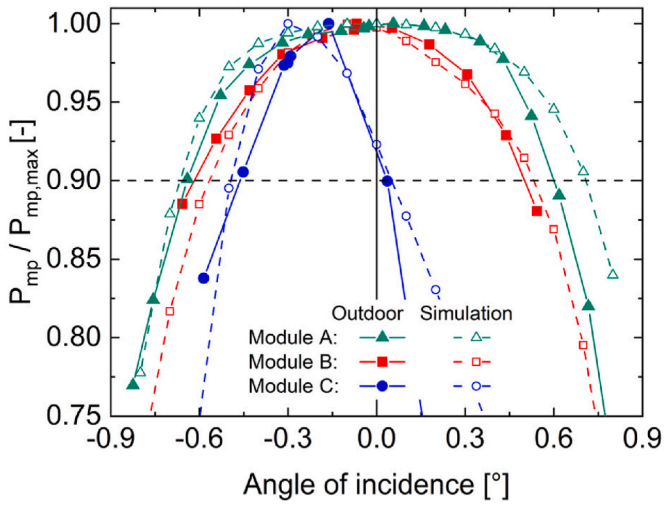

Fig. 4. Acceptance angle data: Measured (closed symbols, solid line) and simulated (open symbols, dashed line) normalized power output P_{mp} as function of the angle of incidence in x-direction. Modules A, B, C (green/triangle, red/square, blue/circle) vary in their mean radial displacement of the SOE, being 20 µm, 115 µm, and 237 µm, respectively.

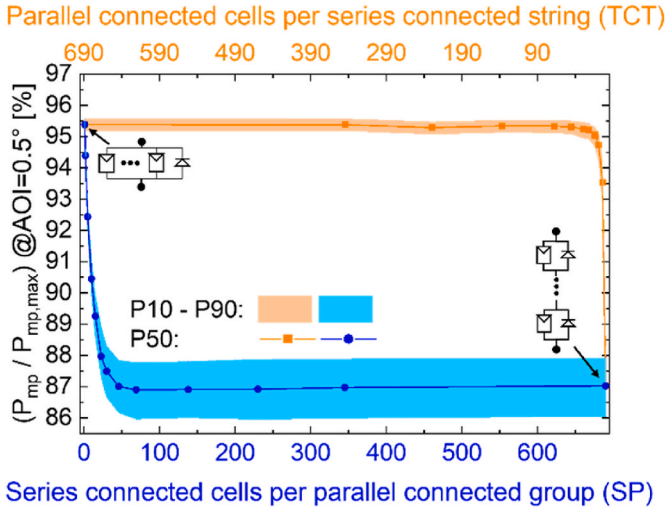

Fig. 5. Relative power normalized to the maximum power $P_{mp}/P_{mp,max}$ as function of two electrical interconnection configurations: total-cross-tied (orange, square) or series-parallel (blue, circle). For every configuration 500 modules were simulated with random combined cell currents from the reference case at $AOI = 0.5°$.

largely hits the active PV cell area. At tilted incidence, however, the situation changes: Fig. 5 shows the power output at $AOI = 0.5°$ normalized to the power of the design case for the two electrical interconnection configurations. In the TCT configuration (orange), the number of parallel connected cells per series connected strings is increased and in the SP configuration (blue), the number of series connected cells per parallel group is increased.

The power output varies between 95.5 $\%_{rel}$ for purely parallel connection and 86.9 $\%_{rel}$ for purely series connection. In the TCT configuration, for long parallel groups only marginal influence by the number of cells in parallel is observed, whereas for shorter parallel groups the power drops noticeably at length below 30 cells.

In the SP configuration, connecting two cells in series within a string result in a power loss of 1.1 $\%_{rel}$, compared to a purely parallel connection. The power continues to decrease until 46 cells are connected in series within a string. Then, with more cells connected in series within a string, the median power output remains at 87 $\%_{rel}$.

The power loss associated with a higher number of series connected cells per parallel group increases due to a reduction in fill factor. When solar cells with varying individual currents are connected in series and connected to a bypass diode, the short-circuit current remains unaffected. However, the current-voltage curve exhibits multiple steps in current, resulting in a decrease in fill factor.

In practice, a purely parallel connection within a module is not reasonable due to high currents and the risk of thermal runaway [10]. Higher currents result in additional series resistance losses [22] or require more or thicker wiring and cabling. Therefore, a combination of parallel and series connections is preferred. Comparing the two configurations, TCT yielded higher performance compared to SP. These findings are consistent with those reported by Steiner et al. [10].

The selection of the number of cells connected in parallel should be based on the current distribution. Assuming tracking accuracy is better than the studied case of $AOI = 0.5°$, for the given tolerances, an electrical interconnection of 30 cells in parallel and 23 groups in series yields almost the same performance as a purely parallel interconnection ($\Delta P10 = 0.23\ \%_{abs}$, $\Delta P50 = 0.14\ \%_{abs}$). Conversely, a tracking accuracy worse than $AOI = 0.5°$ results in increased current scattering and requires a higher number of parallel connected cells. Note that for operating a power plant energy yield in kWh/year would be the more relevant metric. But such a calculation [23] would require additional data such as irradiance, spectrum, temperature, as well as also the tracking accuracy, particularly a representative distribution of *AOIs*.

3.1.2. Acceptance angle

For the operation of a power plant, the acceptance angle of a CPV module is an important parameter, as it stresses or relaxes requirements on the tracking accuracy. For a given tracking system the acceptance angle has a high influence on the actual module performance in the field. We apply our model to analyze the influence of different electrical interconnections on the acceptance angle of our micro-CPV module with the specific tolerance distributions of the reference case.

Fig. 6 illustrates how the interconnection scheme affects the acceptance angle. The statistical data of the nested Monte-Carlo model is shown for the three cases purely parallel "690p1s" (orange), purely series "1p690s" (green), and the TCT combination of 30 parallel and 23 series interconnection "30p23s" (blue). The respective acceptance angles (power> 90 %) $\alpha_{90\%,Pmp}$ related to the 10th, 50th and 90th percentiles (P10/P50/P90) are highest for the 690p1s case with $\alpha_{90\%,Pmp} =$ 0.63°/0.64°/0.64°, but nearly equal for the 30p23s case with $\alpha_{90\%,Pmp} =$ 0.62°/0.63°/0.64°, while being lowest for the 1p690s case with $\alpha_{90\%,Pmp} =$ 0.39°/0.42°/0.45°. Additionally, the 1p690s case exhibits the highest scattering. Note, these percentiles are defined as probability of non-exceedance, meaning that 90 % of the samples are above the P10 value, while 10 % are above the P90 value.

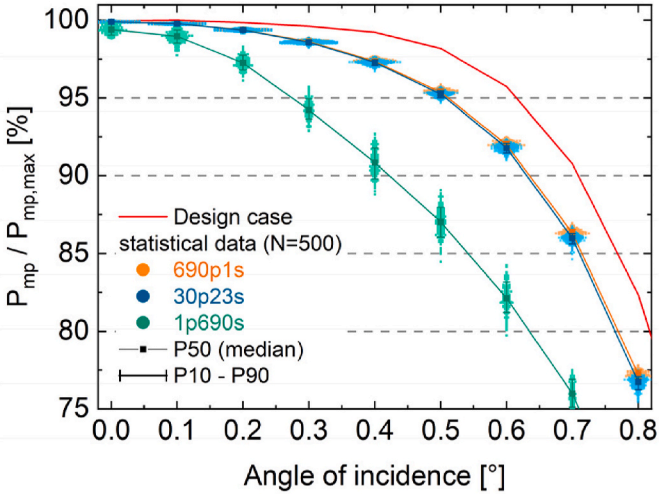

Fig. 6. Relative power $P_{mp}/P_{mp,max}$ as a function of the *AOI* for different interconnection schemes: purely parallel "690p1s" (orange), purely series "1p690s" (green) and a combination of 30 parallel and 23 series connection "30p23s" (blue). Based on the statistical data, the 50th percentile (square) and 10th to 90th percentiles (error bar) are presented. In addition, the design case (red line) with ideal components and alignment is visualized.

It is remarked that the 10th percentile, which represents the worst 10 %, of the statistical data, has a larger acceptance angle for 690p1s and 30p23s than P10 of single cell-lens units with 0.5° reported in Ref. [9]. It differs by 0.13° and 0.12° for 10 % relative current loss, respectively. This highlights how (partially) parallel connected cells effectively mitigate the inferior performance of single cell-lens units by averaging out their variations and thereby reducing the effect of lower outliers.

3.2. Sensitivity analysis: required precision of tolerances

After having analyzed the influence of tolerances on the module performance and optimization of the interconnection scheme, as a next step we quantitatively evaluate the impact of individual tolerances on performance separately in an inverse fashion. This is important to determine how performance behavior responds to variations in tolerances. The metric of interest is the change in performance relative to each tolerance alteration ($\Delta P_{mp}/\Delta\sigma_i$).

We use the procedure of the two-step nested Monte-Carlo approach as described in section 2. We start from the reference case and consider *AOIs* of 0° and 0.5°. The reference case serves as a baseline, and we incrementally adjust one tolerance distribution individually by changing the assumed value for its standard deviation σ_i. We consider a full 690-cell module with all cells connected in parallel. The adjustment of one tolerance distribution is repeated until the power loss attains a threshold of either 5 % or 10 %. This procedure is conducted for all tolerance distributions. Fig. 7 illustrates the result of this procedure for the example of the lateral displacement of the solar cell (cell *x,y*). For each

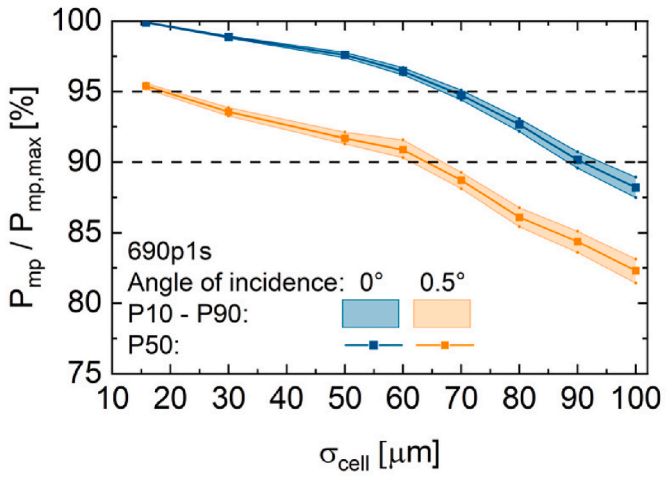

Fig. 7. Power normalized to the power of the design case as a function of the normal distribution of the lateral displacement of the solar cell σ_{cell}. All other tolerances remain within the measured tolerance distributions (reference case) $\sigma_{i,reference}$. The angle of incidence is either 0° (blue) or 0.5° (orange) and the modules consist of 690 cells and are purely parallel interconnected.

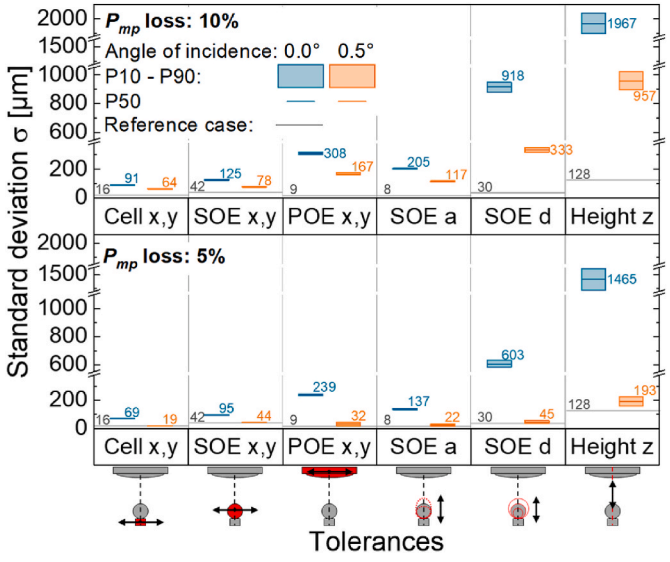

Fig. 8. Sensitivity analysis: Maximum standard deviation for each tolerance resulting in a 5 % and 10 % (bottom and top graph, respectively) power drop compared with the design case. The values for all other tolerances are defined by the reference case (gray line). The cases for an *AOI* of 0° (blue) and 0.5° (orange) are plotted.

tolerance distribution and *AOI*, 500 modules are modeled. The intersections of the modeled curves with $P_{mp}/P_{mp,max}$ at 90 % and 95 % lead to certain tolerance distributions, which are plotted in Fig. 8.

Fig. 8 shows the standard deviation σ for all six tolerances, namely the lateral displacements of cell, SOE, and POE, vertical displacement between the base plate and POE, the deviation in the SOE diameter and the SOE roundness, to achieve $P_{mp}/P_{mp,max}$ losses of 5 % and 10 % for an *AOI* of 0° (blue) and 0.5° (orange). Note, the standard deviation presents a normal distribution, meaning that 68.2 % of the displacements fall within the calculated tolerance. The maximum tolerance for single displacements can still be higher to achieve performances above the specific threshold.

The analysis shows that the cell position, followed by the spherical lens position has the smallest tolerance distribution to restrain a power loss below 5 % or 10 % and, thus, are the most crucial tolerances. Then, the sensitivity follows the order: roundness of the spherical lens, lateral position of the primary lens, diameter of the spherical lens and then the height. A discussion of the underlaying causes for these behaviors is given in the Appendix, where case studies are presented in which individual tolerances in single cell-lens units are varied and the resulting flux profiles are analyzed.

It is interesting to note that if the acceptable loss compared with the design case is increased from 5 % to 10 %, the acceptable tolerances increase by a factor between 1.3 (cell *x,y*) and 1.5 (SOE *d*) for an *AOI* of 0°. For an *AOI* of 0.5°, the tolerances increase by a factor between 1.7 (SOE *x,y*) and 6.2 (SOE *d*).

4. Conclusion

Tolerances are ubiquitous in manufacturing. As the number of statistically independent tolerances increases, the complexity of analyzing their collective impact on performance quickly rises. To overcome this complexity, we introduced a novel method to quantitatively evaluate the influences of individual tolerances in the presence of others using a two-step nested Monte-Carlo approach.

This method was applied on the micro-CPV module developed at Fraunhofer ISE to study the influence of eight tolerances on the power output of panel (24" × 18")-sized 690-cell modules, considering the angle of incidence and electrical interconnection. In a module we observe different behavior than in single cell-lens units: Considering a reference case based on experimental tolerance distributions, we found that for 90 % of the cases, the acceptance angles $\alpha_{90\%,Pmp}$ for 10 % power loss increase by 0.13° for purely parallel connection compared to single cell-lens units. In purely parallel connected modules, the current variation among single cells is fully compensated. As purely parallel connection is impractical, we determine the number of parallel connected cells in a partially parallel interconnection (TCT configuration) to still achieve high module power. Here, the median acceptance angle of 0.63° for 30 cells in parallel and 23 in series connection approaches that of a purely parallel interconnection, which is 0.64°.

In the field of product development and optimization for emerging technologies, it is crucial to assess various optimization potentials in terms of both improvement possibilities and the costs associated with potential developments. This model allows the quantitative assessment of tolerance distributions, acceptance angles, and electrical interconnections, thereby guiding future research and development efforts towards the areas with the most significant impact. Additionally, it provides a basis for techno-economic optimization and manufacturing decisions, balancing the need for precision against cost considerations.

Overall, this study not only introduces a novel analytical tool but also strategically informs product development and manufacturing processes. This could potentially accelerate technological advancement and commercial success in new markets. For the investigated micro-CPV module, the assembly of the solar cell and the SOE are the most critical manufacturing processes.

CRediT authorship contribution statement

Elisa Kaiser: Writing – original draft, Visualization, Validation, Methodology, Formal analysis, Conceptualization. **Maike Wiesenfarth:** Writing – review & editing, Conceptualization. **Peter Schöttl:** Writing – review & editing, Software, Methodology. **Marc Steiner:** Writing – review & editing, Software. **Stefan W. Glunz:** Supervision. **Henning Helmers:** Writing – review & editing, Supervision, Methodology, Funding acquisition, Conceptualization.

Declaration of competing interest

The authors declare that they have no known competing financial interests or personal relationships that could have appeared to influence the work reported in this paper.

Acknowledgment

The authors thank A. Dilger, A. Bösch and T. Dörsam at Fraunhofer ISE for support with the module manufacturing, P. Nitz and F. Dimroth for valuable discussions. We acknowledge M. Knausenberger and EVY-TRA GmbH for providing circuit boards on glass, F. Klotz, R. Löckenhoff, V. Khorenko and AZUR SPACE Solar Power GmbH for providing five-junction solar cells, S. Lehmann, A. Wölfel and SIGMUND LINDNER GmbH for providing spherical glass lenses, M. Voitel, T. Braun and Technische Universität Berlin for assembling the spherical lenses, S. Mehrafsun and Wagenbrett GmbH & Co. KG for the balling process. This work was funded by the German Federal Ministry for Economic Affairs and Climate Action (BMWK) under the "micro-CPV" project (#03EE1046A).

Appendix

A. Analyzing the Underlying Causes of P_{mp} Behavior in the Monte-Carlo Model

In this section we investigate the physical origins of the behavior found in the statistical analysis, focusing on how the light spot changes with geometrical deviations.

Three effects are observed in a cell-lens unit when tolerances are applied: Lateral displacement of either the cell or the concentrated light spot, and changes in the flux profile. The peak-to-average ratio *PAR* measures the uniformity of a flux profile. A higher *PAR* signifies a more concentrated light distribution with more pronounced peaks of intensity. Generally lower *PAR* is desirable as higher *PAR* requires higher peak tunnel current densities. Concentration peaks can lead to uneven heating and localized hot spots, potentially increasing the risk of thermal stress and degradation of the solar cell materials [24]. It can also cause a non-uniform photo-response, where different parts of the cell generate varying amounts of electricity, potentially impacting the overall module efficiency and performance.

In the design case (see Figure 9a), wherein components are perfectly aligned, and the geometry is ideal, all rays that hit the POE surface are concentrated and impinge on the cell surface. Lateral displacement of the cell results in a direct loss of rays as the cell moves out of the concentrated light spot (see Figure 9b). This displacement has the highest impact on P_{mp}, as demonstrated earlier.

Lateral shifts in concentrated light occur when either the SOE or the POE is displaced laterally. Figure 10a and b illustrate the flux profiles for the design case and for a SOE shifted by 100 μm in x-direction, respectively. The dashed lines visualize the boundaries of the concentrated light profile along the x-axis. From Figure 10a to b the concentrated light shifts approximately 75 μm. Consequently, when the SOE is laterally displaced, the flux profile correspondingly shifts, though not proportionally (1-to-1), but rather at a reduced ratio of approximately 1-to-0.75. To incur a 10 % loss in P_{mp}, the lateral displacement of the primary lens can be up to twice that of the SOE. This significant allowance for displacement is enabled by the utilization of a spherical lens. The SOE captures the displaced rays due to the diameter of 1.6 mm and redirecting them toward the cell surface.

Changes in *PAR* occur if the roundness of the SOE varies, its diameter changes or the distance between POE and the baseplate varies. Figure 10c and d depict the flux profile for a compressed and elongated spherical lens, respectively, with a variation of ±100 μm. Compression results in a higher *PAR* of 7.2, while elongation leads to a more homogenized profile with a *PAR* of 2.0. Although for the electrical performance a lower *PAR* is preferable, a lower *PAR* increases the sensitivity to component misalignment. The *PAR* changes with variation in the diameter of the spherical lens or the distance between the lens and base plate, though the degree of these changes varies. Figure 10e–h illustrates the effects on *PAR* for diameter deviation of ±200 μm resulting in *PARs* of 3.8 and 2.7, and for height deviations of ±1 mm resulting in *PARs* of 5.6 and 2.0.

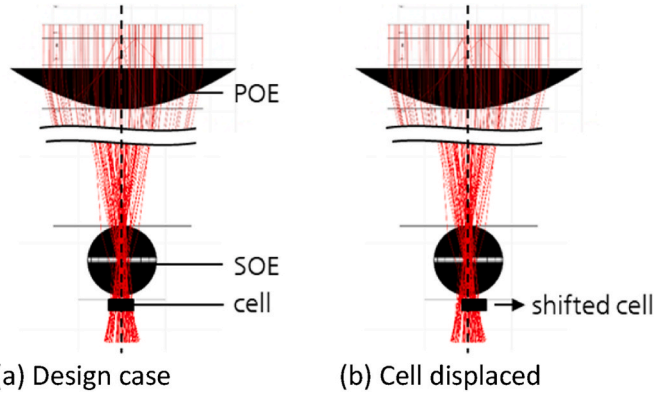

Fig. 9. Sketch of the optical model. a) Design case: All rays hit the solar cell surface. b) Cell is displaced: Some rays are lost due to the shifted cell.

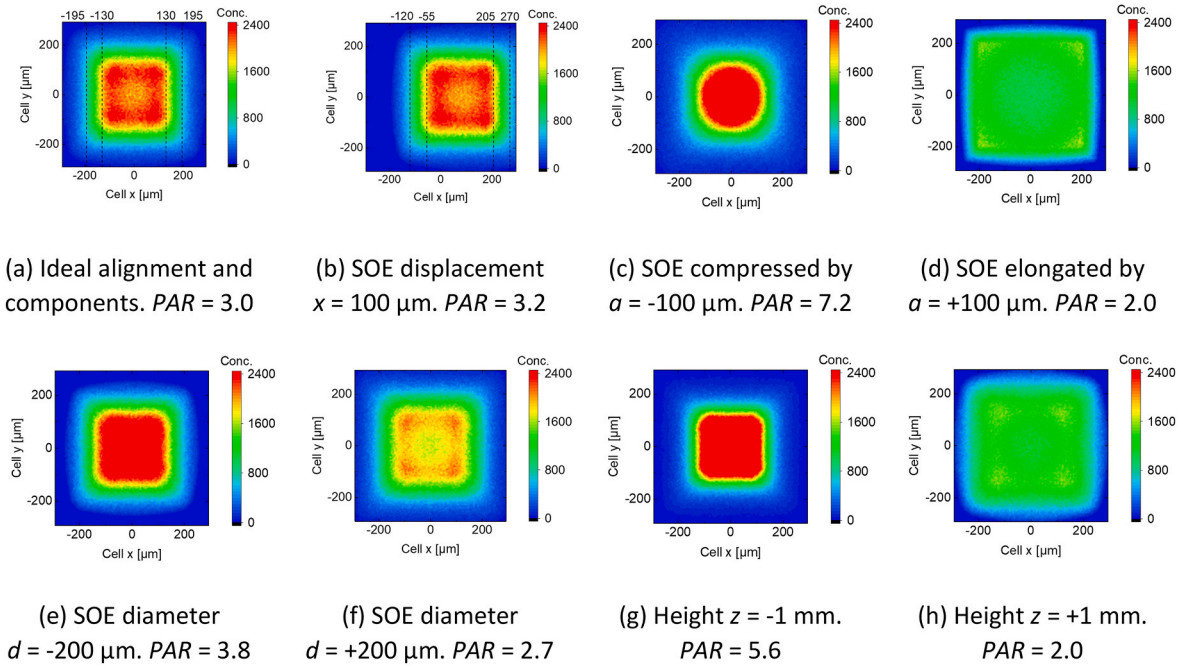

Fig. 10. Flux profile of single tolerances, all other tolerances are assumed to be ideal.

Data availability

The data that has been used is confidential.

References

[1] E. Kaiser, M. Wiesenfarth, V. Vareilles, M. Schneider-Ramelow, S.W. Glunz, H. Helmers, Forced motion activated self-alignment of micro-CPV solar cells, IEEE J. Photovoltaics 14 (2) (2024) 288–295.

[2] S. Paap, V. Gupta, A. Tauke-Pedretti, P. Resnick, C. Sanchez, G. Nielson, J.L. Cruz-Campa, B. Jared, J. Nelson, M. Okandan, W. Sweatt, Cost analysis of flat-plate concentrators employing microscale photovoltaic cells for high energy per unit area applications, in: IEEE 40th Photovoltaic Specialist Conference (PVSC), 2014, pp. 2926–2929. Denver, Colorado, USA.

[3] M. Wiesenfarth, I. Anton, A.W. Bett, Challenges in the design of concentrator photovoltaic (CPV) modules to achieve highest efficiencies, Appl. Phys. Rev. 5 (4) (2018) 41601.

[4] C. Domínguez, N. Jost, S. Askins, M. Victoria, I. Antón, A review of the promises and challenges of micro-concentrator photovoltaics, in: AIP Conf. Proc. CPV-13, 2017 80003. Ottawa, Canada.

[5] N. Jost, T. Gu, J. Hu, C. Domínguez, I. Antón, Integrated micro-scale concentrating photovoltaics: a scalable path toward high-efficiency, low-cost solar power, Sol. RRL 7 (16) (2023) 2300363. https://onlinelibrary.wiley.com/doi/full/10.1002/solr.202300363.

[6] E. Kaiser, P. Schöttl, M. Wiesenfarth, P. Nitz, H. Helmers, Effects of manufacturing tolerances on micro-CPV module performance, in: AIP Conf. Proc. CPV-18, 2023 30002. Miyazaki, Japan.

[7] A. Ritou, P. Voarino, B. Goubault, N. David, S. Bernardis, O. Raccurt, M. Baudrit, Mechanical tolerances study through simulations and experimental characterization for a 1000X micro-concentrator CPV module, in: AIP Conf. Proc. CPV-13, 2017 30007. Ottawa, Canada.

[8] E. Menard, M. Sullivan, J. Wilson, B. Fisher, S. Seel, M. Meitl, K. Ghosal, S. Burroughs, Optics development for micro-cell based CPV modules, in: High and Low Concentrator Systems for Solar Electric Applications VI, 2011 810805. San Diego, California.

[9] E. Kaiser, M. Wiesenfarth, P. Schöttl, M. Steiner, S.W. Glunz, H. Helmers, Effect of manufacturing tolerances on micro-CPV assemblies: A quantitative approach based on statistical modeling, Sol. Energy Mater. Sol. Cells. https://doi.org/10.1016/j.solmat.2024.113256.

[10] M. Steiner, G. Siefer, A.W. Bett, An investigation of solar cell interconnection schemes within CPV modules using a validated temperature-dependent SPICE network model, Progress in Photovoltaics 22 (5) (2014) 505–514. https://onlinelibrary.wiley.com/doi/full/10.1002/pip.2284.

[11] P. Schöttl, G. Bern, P. Nitz, F. Torres, L. Graf, Raytrace3D by Fraunhofer ISE: Accurate and Efficient Ray Tracing for Concentrator Optics, Fraunhofer Institut für Solare Energiesysteme ISE, 2022 [Online] Available: https://www.ise.fraunhofer.de/content/dam/ise/de/downloads/pdf/raytrace3d.pdf. (Accessed 20 May 2022).

[12] R. Branke, A. Heimsath, Raytrace3D-Power tower - a novel optical model for central receiver systems, in: *16th SolarPACES Conference*, Perpignan, France, 2010.

[13] Linear technology, SwitcherCAD III/LT-Spice Manual.

[14] K.C. Reinhardt, Y.K. Yeo, R.L. Hengehold, Junction characteristics of Ga0.5In0.5P n + p diodes and solar cells, J. Appl. Phys. 77 (11) (1995) 5763–5772.

[15] Y.P. Varshni, Temperature dependence of the energy gap in semiconductors, Physica 34 (1) (1967) 149–154. https://www.sciencedirect.com/science/article/pii/0031891467900626.

[16] H. Helmers, C. Karcher, A.W. Bett, Bandgap determination based on electrical quantum efficiency, Appl. Phys. Lett. 103 (3) (2013).

[17] ASTM G173-03, Standard Tables for Reference Solar Spectral Irradiances: Direct Normal and Hemispherical on 37° Tilted Surface, 2008.

[18] A. Neumann, A. Witzke, S.A. Jones, G. Schmitt, Representative terrestrial solar brightness profiles, J. Sol. Energy Eng. 124 (2) (2002) 198–204.

[19] P. Schroth, R. Löckenhoff, D. Fuhrmann, M. Meusel, A. Frey, M. Steiner, G. Siefer, AZUR's new 5C46 CPV cell: final design for optimized outdoor performance, in: AIP Conf. Proc. CPV-17, Germany/Online, Freiburg, 2022 20008.

[20] M. Wiesenfarth, D. Iankov, J.F. Martínez, P. Nitz, M. Steiner, F. Dimroth, H. Helmers, Technical boundaries of micro-CPV module components: how small is enough?, in: AIP Conf. Proc. CPV-17 Germany/Online, Freiburg, 2022 30008.

[21] IEC 62670-3, Concentrator Photovoltaic (CPV) Performance Testing - Part 3: Performance Measurements and Power Rating, 2013. Geneva, Switzerland.

[22] M. Steiner, J. Medvidovic, G. Siefer, A.W. Bett, F. Dimroth, S. Kurtz, G. Sala, Increasing the energy yield of CPV modules through optimized solar cell interconnection, in: AIP Conf. Proc. CPV-7, 2011, pp. 404–408. Las Vegas, Nevada, (USA).

[23] M. Steiner, G. Siefer, T. Hornung, G. Peharz, A.W. Bett, YieldOpt, a model to predict the power output and energy yield for concentrating photovoltaic modules, Prog. Photovoltaics Res. Appl. 23 (3) (2015) 385–397.

[24] H. Baig, K.C. Heasman, T.K. Mallick, Non-uniform illumination in concentrating solar cells, Renew. Sustain. Energy Rev. 16 (8) (2012) 5890–5909. https://www.sciencedirect.com/science/article/pii/S1364032112004133.